ChemComm

Accepted Manuscript

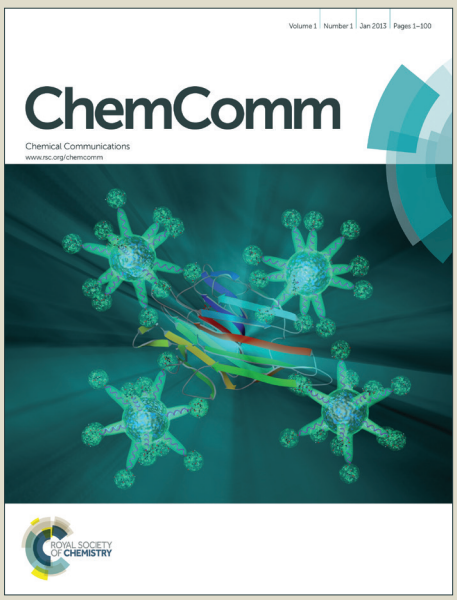

ROYAL SOCIETY OF CHEMISTRY

www.rsc.org/chemcomm

Journal Name

COMMUNICATION

In Situ Observation of Sodiation Process in CuO Nanowires

Huihui Liu,‡[a] Fan Cao,‡[a] He Zheng,‡[a] Huaping Sheng,[a] Lei Li,[a] Shujing Wu,[a] Chun Liu,[a] and Jianbo Wang*[a]

Received 00th January 20xx,
Accepted 00th January 20xx

DOI: 10.1039/x0xx00000x

www.rsc.org/

In this study, aided by the *in situ* transmission electron microscopy, we observe the dynamic morphology evolution and phase transformations of CuO nanowires during sodiation. Our results facilitate the fundamental understanding of the sodiation mechanism of CuO nanostructures as the electrode materials in sodium-ion battery.

Sodium ion batteries (SIBs) have recently obtained great attentions, motivated by the vast demand in the rechargeable battery market and the rapid development of lithium ion batteries (LIBs).[1-4] Compared with LIBs, the price of SIBs should be lower owing to the abundant natural storage of sodium, which can satisfy the demand for large-scale energy storage in applications from electronic vehicles to power backup.[5] Nonetheless, despite that the chemical properties of sodium are similar to those of lithium, both the ionic radius and molar mass of sodium are larger than those of lithium. Thus, it is more difficult for sodium to reversibly react with the electrode materials, leading to different reaction mechanisms and performance.[6-8] It is reported that the sodiation processes of the oxides and fluorides are extremely irreversible compared with the corresponding lithiation processes.[8, 9]

In order to select suitable electrode materials for SIBs, many electrode materials of LIBs have been applied in the study of the SIBs, such as Fe_2O_3,[10] SnO_2,[11] and Sn.[12] CuO is a promising electrode material due to its abundance, reasonable price, nontoxicity, and high theoretical capacity of 674 mA h g^{-1}. Meanwhile, CuO has been demonstrated as an anode material in the SIBs.[13] It was documented that the binder free porous CuO rod arrays grown on the copper (Cu) foil had superior electrochemical performance and the capacity of 640 mA h g^{-1} even at high current density of 200 mA g^{-1}.[14] Generally, it is easy to acquire the performance parameters of an electrode material by the measurement of galvanostatic charge-discharge and cyclic voltammetry curves of an assembled coin-cell.[15] However, the intermediates and morphology evolution of electrode materials during the discharge-charge processes, which are closely associated with the cycling efficiency and capacity storage of rechargeable batteries, are still obscure.[8, 11, 12] As such, it is of necessity to investigate the real-time microstructure and composition evolution during the period of the electrochemical reactions.

Enlightened by the recent advent of *in situ* transmission electron microscopy (TEM) which has been proved to be an effective technique to observe the microstructural evolution and phase transformations of nanomaterials in the presence of external fields,[16-20] the dynamic lithiation or sodiation behaviors of electrode materials can be obtained by *in situ* TEM.[21-23] In this study, the real-time sodiation behavior of CuO nanowires (NWs) was directly visualized in the nanosized solid cell. The experiment was performed inside the JEOL JEM-2010 FEF (UHR) electron microscope operated at 200 kV.

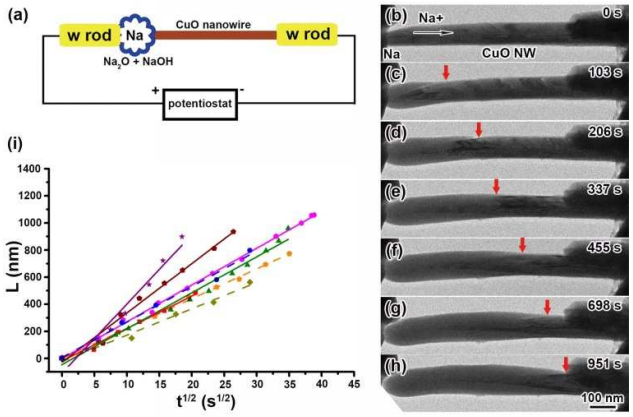

Fig. 1 (a) Schematic illustration of the *in situ* experimental setup. (b-h) Time-lapsed images illustrating the morphology evolution of a CuO NW at the applied voltage of -3 V during first sodiation. (i) Plots of the sodiated length versus the square root of the reaction time for eight CuO NWs with (solid lines) and without e-beam irradiation (dashed lines) during sodiation.

Monoclinic CuO NWs were synthesized by the conventional method by simply heating Cu grids at above 400 °C as reported previously.[24] Fig. 1(a) presents the schematic illustration of the

[a] *School of Physics and Technology, Center for Electron Microscopy and MOE Key Laboratory of Artificial Micro- and Nano-structures, Wuhan University, Wuhan 430072, China. Email: wang@whu.edu.cn*

† Electronic Supplementary Information (ESI) available: Supporting video and figures information. See DOI: 10.1039/x0xx00000x

‡ These authors contributed equally.

assembled nanosized SIB open-cell that enables the electrochemical experiments of CuO NWs. The system was consisted of the CuO NW as the working electrode, bulk sodium (Na) metal on the tungsten (W) rod as the counter electrode, and a solid electrolyte of naturally grown sodium oxide and hydroxide (Na_2O + NaOH) on the Na metal.[12] The working and counter electrodes of the nanosized SIB were fixed onto the Nanofactory EP1000 TEM-scanning tunneling microscopy (STM) platform inside the glovebox (water and oxygen concentrations both below 0.1 ppm) and sealed with a plastic tube filled with dry argon and then transferred into the TEM column. During the experiments, the counter electrode could be driven to touch the CuO NWs aided by the piezo-positioner. Potential of -3 V or -4 V was applied to the working electrode with respect to the counter electrode to facilitate the sodiation of the CuO NW.

Time-lapsed images shown in Figs. 1(b)-1(h) present the typical morphology evolution of a single CuO NW during sodiation (see Video S1(ESI†)). The pristine length of the CuO NW is nearly 1000 nm. It is evident that the reaction front (marked by the red arrows) keeps a conical morphology during the whole process, suggesting that the sodiation proceeds from the surface to the center of the NW. With the reaction front passing by, the axial elongation of the CuO NW is not obvious while the expansion along the radial direction is nearly 27%, implying the anisotropic sodiation mechanism. During the whole reaction process, no fracture or cracking appeared.

To gain a better understanding of the sodiation process, Fig. 1(i) presents the plots of the sodiated length (L) versus the square root of the reaction time ($t^{1/2}$) for 8 CuO NWs. Obviously, L are proportional to ($t^{1/2}$) (*i.e.* $L \propto t^{1/2}$), indicating that the sodiation mechanism is controlled by the long-ranged diffusion transport along the whole NW inside such a solid-cell configuration, rather than the short-ranged processes near the reaction front (*i.e.* $L \propto t$).[25] The five solid lines represent the sodiation results with e-beam irradiation while the three dashed lines depict the sodiated results with limited e-beam irradiation. To be specific, in the latter case, once the CuO NW contacted with the counter electrode, we blanked the beam and then applied a potential to the working electrode, taking images by intermittently turning on the beam for about 5 seconds per 3-5 minutes. Meanwhile, both experiments were carried out under extremely low e-beam intensity (10^{-2}-10^{-1} A cm^{-2})[26] to minimize the influence of e-beam irradiation. It is reasonable that the electrons (e^-) could intervene the sodiation (Na^+). Nevertheless, the consistent results indicate that the influence of e-beam on the sodiation mechanism of CuO NWs is not crucial.

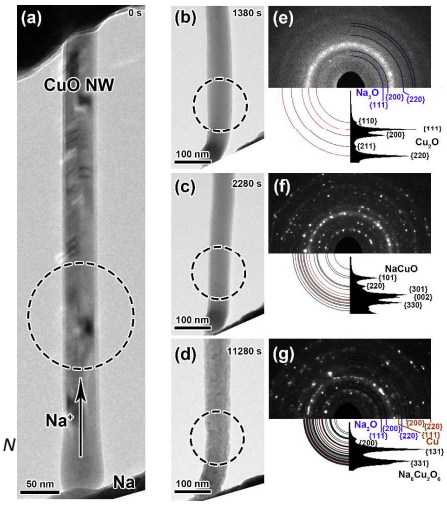

Fig. 2 (a) TEM image of a pristine CuO NW. (b-d) TEM images of the sodiated CuO NW circled in (a). (c-e) Electron diffraction (ED) patterns of the circled area in (b), (c), and (d), respectively.

Consistently, the entire sodiation process can be divided into three steps. Fig. 2(a) presents the pristine morphology of a single CuO NW. Figs. 2(b)-2(d) correspond to the typical TEM images taken from the circled area shown in Fig. 2(a) at different reaction steps, respectively. Firstly, the CuO can be firstly sodiated to Cu_2O (JCPDS No. 77-0199, lattice parameter: a = 4.25 Å) and Na_2O (JCPDS No. 77-2148, lattice parameter: a = 5.55 Å) as revealed by the electron diffraction patterns (Fig. 2(e)), in agreement with the previous report. In subsequence, the products were converted to NaCuO (JCPDS No. 77-1699, lattice parameter: a = 8.86 Å, c = 4.66 Å) (Fig. 2(f)). Finally, the fully sodiated products were mainly consisted of $Na_6Cu_2O_6$ (JCPDS No. 79-0320, lattice parameter: a = 10.94 Å, b = 12.03 Å, c = 16.38 Å), Na_2O, and Cu (JCPDS No. 04-0836, lattice parameter: a = 3.61 Å). The full sodiation products of CuO are $Na_6Cu_2O_6$, Na_2O and Cu, which is similar to the electrode material of FeF_2 that can be sodiated to Na_3FeF_6, Fe and Na_2O.[8] The detailed reaction processes can be expressed as follows:

$$2CuO + 2Na^+ \rightarrow Cu_2O + Na_2O \quad (1)$$

$$Cu_2O + Na_2O \rightarrow NaCuO \quad (2)$$

$$7NaCuO + Na^+ \rightarrow Na_6Cu_2O_6 + Na_2O + 5Cu \quad (3)$$

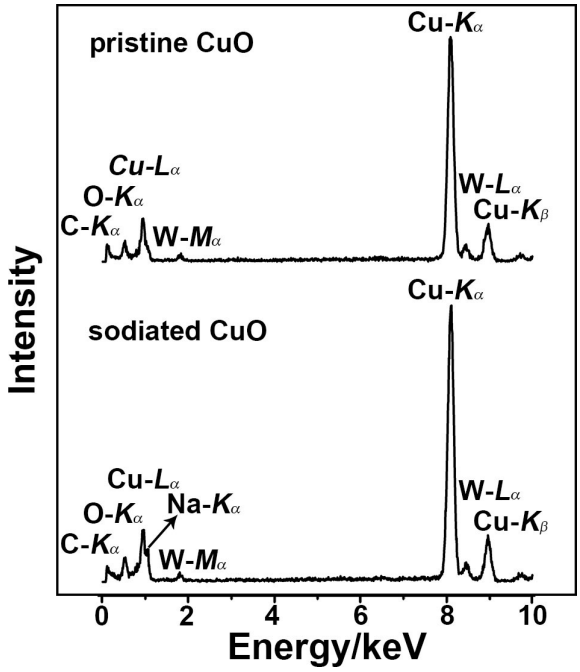

Fig. 3 EDS spectra of pristine and sodiated CuO NWs.

In order to accurately identify the sodiation phases, high resolution transmission electron microscopy (HRTEM) images (Fig. S1(ESI†)) from two different sodiated CuO NWs were acquired during the second (Figs. S1(a)-S1(b)) and third sodiation stages (Figs. S1(c)-S1(f)). However, since the images was obtained with focused e-beam (10^1-10^2 A cm^{-2}) which might heat the NWs remarkably[27] and thus facilitate the second stage reaction (*i.e.* $Cu_2O + Na_2O \rightarrow$ NaCuO (310 °C)),[28] HRTEM images of Cu_2O and Na_2O formed in the first stage could not be obtained successfully. Nonetheless, it should be noted again that the e-beam with extremely low intensity

(10^{-2}-10^{-1} A cm^{-2}) was applied during the regular structural characterization presented in this paper (*e.g.* Figs. 1-2). As will be discussed later, such low intensity e-beam is not the major driving force for the second stage chemical reaction. Instead, it is believed that the thermal heating is the main driving force for this reaction.[28] During the sodiation process, a constant voltage (-3 V or -4 V) and current was applied on a single Cu NW with low thermal conductivity (20 W/(mK)),[29] which may increase the local temperature of the single NW via Joule-heating.[30] Figs. 3(a)-3(b) present the energy dispersive X-ray spectra (EDS) of pristine and sodiated CuO NWs. The existence of the characteristic peak of Na verifies that the sodium ions indeed react with CuO NW. The signals of C and W originate from the Cu grid and W rod.

Interestingly, Wang et al reported that CuO can be firstly sodiated to Cu_2O and Na_2O which were converted to Cu and Na_2O via the *ex situ* electrochemical study.[31] No NaCuO or $Na_6Cu_2O_6$ phases were found in their experiments. The discrepancy may originate from the different cell configurations. To be specific, in the former work,[31] the liquid electrolyte rather than the solid electrolyte was employed. However, it was reported that the lithiation of Si NWs with solid or liquid electrolytes yield the same products.[25] Future work is required to clarify whether or not the different types of electrolytes may influence the sodiated products. Furthermore, it is noted that in the current work, the sodiation process is directly monitored under a high vacuum condition. In contrast, during the *ex situ* experiments reported in references,[15, 31] it is inevitable that the reaction products would contact with the air, especially when the samples were transferred for the structural investigation (*e.g.* X-ray diffraction, TEM). Additionally, it was reported that the NaCuO is pretty unstable in the air.[32] To confirm this, we have intentionally taken out the TEM holder after the NaCuO phase was formed during the sodiation (Fig. S2(ESI†)). In subsequence, the holder was re-inserted into the TEM chamber. Astonishingly, it was found that NaCuO can be converted to Cu_2O and Na_2O (Fig. S2(ESI†)), suggesting that such phase cannot be easily detected during the *ex situ* experiment. Because both the LIBs and SIBs were operated in the air-free environment, it is of necessity to investigate the structural evolution during the electrochemical reaction under a high vacuum condition. Furthermore, the Cu_2O and Na_2O (Figs. S2(c-d)(ESI†)) did not transform to NaCuO under the long-period e-beam irradiation, which indicated that the e-beam irradiation with extremely low intensity might not exert significant influence on the normal reaction.

In comparison to the *in situ* lithiation results of CuO NWs in solid cells,[33] these results nearly show the discrepancy between sodiation and lithiation reaction.[25] Furthermore, although most of reports assume that it is reasonable to have similar reaction products for sodium ion and lithium ion storage,[34] the inconsistent phenomena between SIBs and LIBs have also been observed in other electrode materials, such as FeF_2[8] and VN.[35] It is believed that electrochemical performance of the electrode is influenced by the diffusion pathway[8] and intermediates[35] depending on the radius of the alkali cations. Therefore, it is unreasonable to only consider sluggish effect on the electrode materials caused by the difference between sodium ion and lithium ion but to pay attention to the varied reaction products and mechanisms to account for the performance discrepancy of CuO electrode materials for SIBs and LIBs.

In summary, the real-time microstructural evolution during sodiation of CuO NWs was directly recorded. Consistently, the sodiation length is proportional to the square root of the reaction time, indicating that the sodiation procedure is controlled by the long-ranged diffusion transport mechanism. Meanwhile, based on the sodiated products, the sodiation process was consisted of three steps, whereas Cu_2O and Na_2O were predominantly formed during the first step. Upon further reaction, the intermediate phase NaCuO nucleated. The final sodiation products were $Na_6Cu_2O_6$, Na_2O, and Cu. It is suggested that the complicated reaction mechanism should be considered for the ongoing relevant exploration of CuO electrode materials applied in the solid cell, such as capacity fading and structure disintegration.

This work was supported by the 973 Program (No. 2011CB933300), the National Natural Science Foundation of China (Nos. 51271134, J1210061), the Fundamental Research Funds for the Central Universities, the CERS-1-26 (CERS-China Equipment and Education Resources System), and the China Postdoctoral Science Foundation (Nos. 2013M540602, 2014T70734).

Notes and references

1. M. D. Slater, D. Kim, E. Lee and C. S. Johnson, *Adv. Funct. Mater.*, 2013, **23**, 947-958.
2. M. Dahbi, N. Yabuuchi, K. Kubota, K. Tokiwa and S. Komaba, *Phys. Chem. Chem. Phys.*, 2014, **16**, 15007-15028.
3. S. W. Kim, D. H. Seo, X. H. Ma, G. Ceder and K. Kang, *Adv. Energy Mater.*, 2012, **2**, 710-721.
4. L. Wang, Z. Xu, W. Wang and X. Bai, *J. Am. Chem. Soc.*, 2014, **136**, 6693-6697.
5. Y. Kim, K. H. Ha, S. M. Oh and K. T. Lee, *Chem. Eur. J.*, 2014, **20**, 11980-11992.
6. V. L. Chevrier and G. Ceder, *J. Electrochem. Soc.*, 2011, **158**, A1011-A1014.
7. B. Huang, K. P. Tai, M. G. Zhang, Y. R. Xiao and S. J. Dillon, *Electrochim. Acta*, 2014, **118**, 143-149.
8. K. He, Y. Zhou, P. Gao, L. Wang, N. Pereira, G. G. Amatucci, K. W. Nam, X. Q. Yang, Y. Zhu, F. Wang and D. Su, *ACS Nano*, 2014, **8**, 7251-7259.
9. M. Valvo, F. Lindgren, U. Lafont, F. Björefors and K. Edström, *J. Power Sources*, 2014, **245**, 967-978.
10. B. Sun, S. J. Bao, J. Le Xie and C. M. Li, *RSC Adv.*, 2014, **4**, 36815.
11. M. Gu, A. Kushima, Y. Shao, J. G. Zhang, J. Liu, N. D. Browning, J. Li and C. Wang, *Nano Lett.*, 2013, **13**, 5203-5211.
12. J. W. Wang, X. H. Liu, S. X. Mao and J. Y. Huang, *Nano Lett.*, 2012, **12**, 5897-5902.
13. F. Klein, B. Jache, A. Bhide and P. Adelhelm, *Phys. Chem. Chem. Phys.*, 2013, **15**, 15876-15887.
14. S. Yuan, X. L. Huang, D. L. Ma, H. G. Wang, F. Z. Meng and X. B. Zhang, *Adv. Mater.*, 2014, **26**, 2273-2279, 2284.
15. L. Li, K. H. Seng, D. Li, Y. Xia, H. K. Liu and Z. Guo, *Nano Res.*, 2014, **7**, 1466-1476.
16. Z. Xu, Y. Bando, W. Wang, X. Bai and D. Golberg, *ACS Nano*, 2010, **4**, 2515-2522.
17. S. Yang, L. Wang, X. Tian, Z. Xu, W. Wang, X. Bai and E. Wang, *Adv. Mater.*, 2012, **24**, 4676-4682.
18. C. Zhang, W. Tian, Z. Xu, X. Wang, J. Liu, S. L. Li, D. M. Tang, D. Liu, M. Liao, Y. Bando and D. Golberg, *Nanoscale*, 2014, **6**, 8084-8090.

19. J. Y. Huang, L. Zhong, C. M. Wang, J. P. Sullivan, W. Xu, L. Q. Zhang, S. X. Mao, N. S. Hudak, X. H. Liu, A. Subramanian, H. Fan, L. Qi, A. Kushima and J. Li, *Science*, 2010, **330**, 1515-1520.
20. H. Zheng, J. Wang, J. Y. Huang, J. Wang and S. X. Mao, *Nanoscale*, 2014, **6**, 9574-9578.
21. Q. Su, D. Xie, J. Zhang, G. Du and B. Xu, *ACS Nano*, 2013, **7**, 9115-9121.
22. Y. Liu, F. Fan, J. Wang, Y. Liu, H. Chen, K. L. Jungjohann, Y. Xu, Y. Zhu, D. Bigio, T. Zhu and C. Wang, *Nano Lett.*, 2014, **14**, 3445-3452.
23. Q. Su, J. Xie, J. Zhang, Y. Zhong, G. Du and B. Xu, *ACS Appl. Mater. Interfaces*, 2014, **6**, 3016-3022.
24. X. C. Jiang, T. Herricks and Y. N. Xia, *Nano Lett.*, 2002, **2**, 1333-1338.
25. X. H. Liu, H. Zheng, L. Zhong, S. Huang, K. Karki, L. Q. Zhang, Y. Liu, A. Kushima, W. T. Liang, J. W. Wang, J. H. Cho, E. Epstein, S. A. Dayeh, S. T. Picraux, T. Zhu, J. Li, J. P. Sullivan, J. Cumings, C. Wang, S. X. Mao, Z. Z. Ye, S. Zhang and J. Y. Huang, *Nano Lett.*, 2011, **11**, 3312-3318.
26. B. Kooi, W. Groot and J. T. M. De Hosson, *J. Appl. Phys.*, 2004, **95**, 924-932.
27. S. Lee, Y. J. Kim, H. J. Lee and H. S. Moon, *J. Am. Ceram. Soc.*, 2001, 84, 2096-2098.
28. A. Möller, *Z. Anorg. Allg. Chem.*, 2005, **631**, 2285-2296.
29. K. Kwak and C. Kim, Korea-Aust. Rheol. J, 2005, **17**, 35-40.
30. H. Zheng, J. Wang, J. Y. Huang, J. Wang, Z. Zhang and S. X. Mao, *Nano Lett.*, 2013, **13**, 6023-6027.
31. L. J. Wang, K. Zhang, Z. Hu, W. C. Duan, F. Y. Cheng and J. Chen, *Nano Res.*, 2014, **7**, 199-208.
32. A. Maljuk, A. B. Kulakov, M. Sofin, L. Capogna, J. Strempfer, C. T. Lin, M. Jansen and B. Keimer, *J. Cryst. Growth*, 2004, **263**, 338-343.
33. X. Wang, D. M. Tang, H. Li, W. Yi, T. Zhai, Y. Bando and D. Golberg, *Chem. Commun.*, 2012, **48**, 4812-4814.
34. X. J. Li, M. M. Hasan, A. L. Hector and J. R. Owen, *J. Mater. Chem. A*, 2013, **1**, 6441-6445.
35. Z. Cui, C. Li, P. Yu, M. Yang, X. Guo and C. Yin, *J. Mater. Chem. A*, 2014, **3**, 509-514.